An Autonomous Underwater Glider with Improved Onboard Navigation for Unattended Mapping

Amy Phung[1,2], Gideon Billings[1,3], Gregory Burgess[1,2], Richard Camilli[1]

***Abstract*— Georeferenced subsurface survey is primarily conducted by autonomous underwater vehicles (AUVs) and remotely operated vehicles (ROVs) that require power-intensive navigation suites, acoustic beacons, and surface support vessels with attendant operations teams onboard. The significant infrastructure required to operate vehicles conducting surveys in remote regions (e.g., under ice) poses increased challenges and remains prohibitively costly, leading to sparse coverage. Unattended operations using autonomous underwater gliders (AUGs) with low power, high-resolution onboard navigation holds promise in scaling up coverage while significantly reducing the operational costs of georeferenced surveys. In this paper, we present a modified AUG equipped with a low power embedded navigation process and results of unattended sonar acoustic surveys using this experimental platform.**

***Index Terms*—Autonomous Underwater Gliders, Field Robots, Marine Robots, Sonar Survey, Under Ice**

I. Introduction

Over three decades have passed since Henry Stommel envisioned a World Ocean Observing System which would utilize a fleet of Slocum floats to record chemical and physical oceanographic measurements throughout the water column while circumnavigating the globe [2]. This observational network of small, long-range, autonomous gliders could map out spatial and temporal features of the global ocean water column and inform pressing scientific questions regarding ocean circulation, the distribution of pollutants, and the trajectory of climate change. Much of Stommel's futuristic vision has been reflected in subsequent decades of oceanographic research, where Autonomous Underwater Gliders (AUGs) have proven their utility for conducting unattended basin-scale surveys that no other man-portable vehicle class can match. In 2009, the Slocum AUG *Scarlet Knight* became the first robot to cross the Atlantic [3], and Slocum AUGs continue to be an integral part of the Ocean Observatories Initiative [4].

This research was supported through National Science Foundation Navigating the New Arctic Grant #1839063, National Ocean Partnership Program Grant #NA19OAR0110408, and the US Department of Energy's Office of Energy Efficiency and Renewable Energy program DE-EE0009801. A. Phung would like to acknowledge financial support from the National Science Foundation Graduate Research Fellowship (No. 2141064), from the National Aeronautics and Space Administration (NASA) through the FINESST program (No. 80NSSC23K1391) and from the Link Foundation Ocean Engineering and Instrumentation Fellowship.

[1]with the Applied Ocean Physics and Engineering Department, Woods Hole Oceanographic Institution, Deep Submergence Laboratory, Woods Hole, MA, USA

[2]with the Massachusetts Institute of Technology, Cambridge, MA, USA

[3]with the Australian Centre for Field Robotics, University of Sydney, NSW, Australia

Contact: rcamilli@whoi.edu

One of the primary challenges in oceanography is collecting measurements that capture both basin-scale dynamics, which inform climate studies, and micro-scale phenomena, which drive biophysical interactions [5]. AUGs are small (i.e., portable by 1-2 people) and can be readily deployed to sample phenomena that are intermittent and localized. Additionally, as a relatively low-cost and long-endurance system, their scalability through multi-vehicle networks makes them a promising solution to achieve the coverage as well as spatial and temporal resolution required for global ocean observation.

AUGs are buoyancy-driven vehicles capable of traversing thousands of kilometers on extremely limited power budgets [6] by adjusting their buoyancy and pitch angle to fly in a sawtooth "yo-yo" vertical profile through the water column while collecting CTD (Conductivity, Temperature, Depth), flow, and turbidity data [2]. Unlike conventional AUVs and ROVs, AUGs are not pitch stable and favor open ocean environments because they lack the navigational accuracy and proximity awareness to safely operate near structures. These attributes make AUGs a challenging platform to use for surveys. Dedicated systems for open ocean exploration are relatively few and tend to be operated in isolation, with each system representing a significant capital investment and ongoing operational expense. For example, the *Sentry* AUV, which operates as part of the National Deep Submergence Facility, conducts over 200 ship-based operational days per year and requires five full-time, at-sea personnel to support deployments and maintenance [7].

While AUGs have proven to be a reliable means of collecting long-range, unattended observations of the water column in open ocean environments, there is pressing scientific need for expanded surveys in confined and operationally challenging environments, such as sub-ice Arctic and Antarctic waters [8]. These regions play critically important roles in global climatic, geological, chemical, and biological processes, yet remain the least studied environments on Earth [9], [10]. Exploration of sub-ice polar environments are logistically challenging and expensive, with ship-based expeditions to some polar regions spaced decades apart [10]. Much of the ice-covered polar oceans are completely inaccessible to all but the most powerful icebreakers, particularly in winter, and research investigation of these regions requires alternative modes of data gathering.

Moorings and ice-tethered platforms have been deployed for many decades to observe ice dynamics and associated seasonal environmental variability, but these systems provide only single point spatial measurements [10], require significant logistical support to deploy and recover, and are often

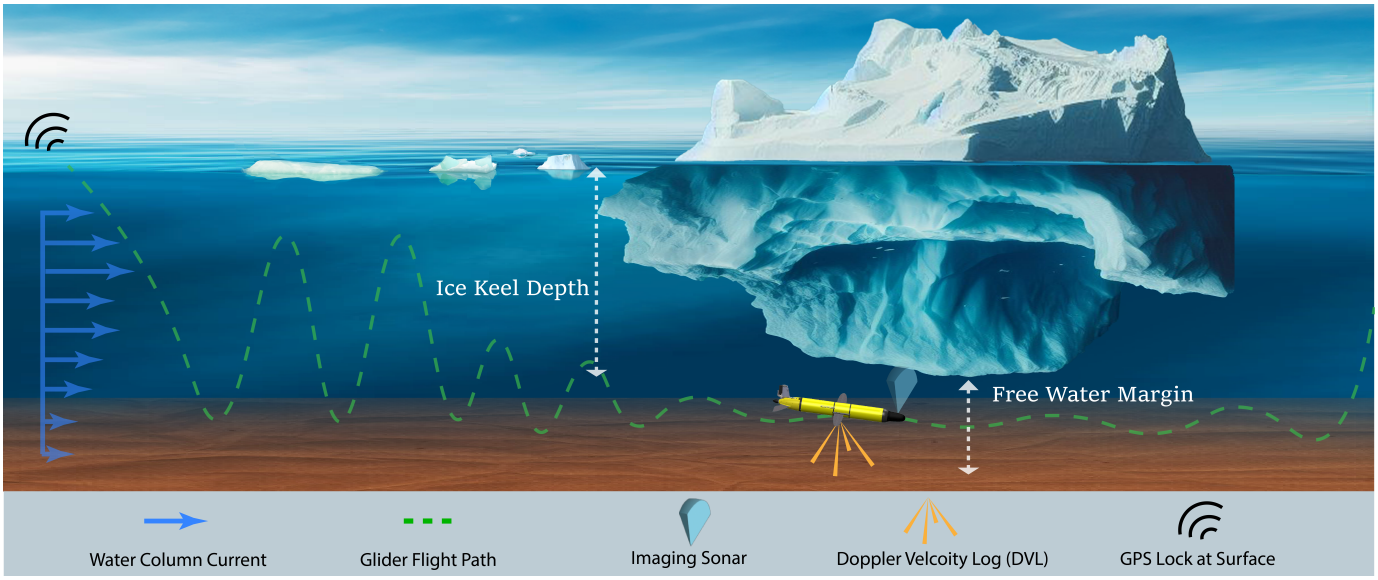

Fig. 1: Our work aims to address the challenges associated with conducting long range surveys under surface-denied environments, such as ice shelves and marginal ice zones. Our modified G3 Slocum Glider is capable of conventional buoyancy driven locomotion for efficient traversal of the open ocean and can seamlessly transition to constant depth "bathtub" profiles for conducting active sensor surveys or transiting across regions with narrow depth constraints. Our real-time DVL-based navigation method [1] can compensate for depth dependent currents, improving the glider's navigation over long ranges when it cannot surface to obtain GPS fixes.

crushed by the ice and destroyed. Under-ice profiling floats are useful for large-scale surveys, but their deployment locations and trajectories are subject to ocean currents [11], limiting their utility for basin-scale investigations. Remotely operated vehicles (ROVs), which are capable of carrying large payloads with a wide variety of scientific instruments and collecting physical samples, have also been deployed for under-ice exploration [12]. However, these vehicles require a significant capital investment and an attendant surface vessel during operations, which in turn increases the logistics and cost. Long-range autonomous underwater vehicles (LRAUVs) offer an attractive means to explore and survey remote open-ocean and sub-ice environments [10], and developing autonomous vehicle platforms with adequate navigation for reliable under-ice operation has been a significant focus of technological research for over 50 years [13]. However, conventional thruster driven AUVs capable of long-range (>1000 km) missions are generally large displacement due to battery capacity requirements, and need significant logistical support for deployment and recovery [6].

In this paper, we present the architecture of an experimental low-power navigation process that we have developed for AUGs which provides georeferenced survey with sufficient accuracy to enable sonar mapping. We demonstrate this utility onboard a highly modified Slocum G3 AUG, *EPIC-DAUG*, by mapping coral reefs in the eastern Caribbean as well as Arctic ice floes with an imaging sonar (Figure 1). This combined navigation and sonar draws less than 15W and fits within the vehicle's form factor, enabling efficient long-range survey without requiring a north-seeking gyro, acoustic beacons, or other external navigation aids.

II. Related Work

Medium displacement AUVs commonly used for benthic or under-ice visual and sonar surveys (e.g., *Sentry* [7] and *Seabed* [14], [15] AUVs), are generally limited in range to ∼10-100 km and require an attendant surface vessel. Some early purpose-built AUVs designed for under-ice navigation were able to extend mission ranges to several hundred km. In 1992, the *Theseus* AUV set a record for autonomous navigation under ice when it laid a fiber optic cable for 200 km in the Canadian Arctic and then returned to the launch station for recovery [16]. The AUV relied on a series of widely spaced acoustic beacons along the flight path for navigation, coupled with an onboard inertial navigation system (INS) and bottom tracking Doppler Velocity Log (DVL). Following this, the International Submarine Engineering (ISE) *Explorer* AUV conducted extensive under-ice seafloor mapping missions in Canada's High Arctic in 2010-2011, utilizing a custom 1500 Hz long-range acoustic homing system in addition to more conventional short-range beacons. The homing beacons were critical to the system design, as the navigation target was an ice camp drifting up to 25 km per day. The vehicle achieved a longest single leg deployment under ice of 320 km.

Autosub is a series of large-class AUVs designed by the National Oceanography Centre in Europe [17], [18], which have a longer range than mid-sized AUVs due to their ability to carry more batteries onboard. The *Autosub Long Range 6000* (ALR6000) has an operational depth rating of 6000 m

and is capable of 2-3 month deployments with a range of up to 1800 km by using high energy-density lithium primary cells [17]. The recently developed ALR1500 is optimized for shallower operations to 1500 m depth and has a theoretical range of 6000 km in a low-power configuration. The vehicle completed a 2000 km transit in May of 2022, consuming only half of its energy capacity. This impressive range is achieved by designing the vehicle for slow speed flight (0.4 m/s) while being neutrally buoyant at the transit depth. The large internal volume and available mass budget of the vehicle supports up to 95 kWhr of lithium primary cell batteries, which is nearly an order of magnitude greater than small displacement vehicles. The long-range Autosub vehicles have enabled collection of critical scientific data in the deep ocean and under glacial ice shelves in the Antarctic [19]. The primary limitation of these vehicles is their large size, which necessitates significant infrastructure for deployment and recovery from ship or shore. The engineering, material, and component cost of building large-class vehicles also limits their scalability to multi-vehicle operations.

The *Tethys* long range AUV [20], developed by the Monterey Bay Aquarium Research Institute (MBARI), is a propeller-driven, small-class vehicle (2 m long, 120 kg displacement) that can achieve basin scale ranges, demonstrated to 1800 km, and operate for weeks at a time to a depth limit of 1500 m. The vehicle design utilizes many elements of underwater gliders, including ultra-low-power computers, an internal moving mass to tune pitch, a buoyancy drive to adjust the ballast for efficient neutral buoyancy flight, and transit speeds ranging from 0.5 to 1.0 m/s. The main difference between Tethys and a hybrid glider is that Tethys relies on thruster-powered locomotion and cannot utilize its buoyancy drive alone.

Seaglider is an AUG designed for high-endurance low-speed flight [21], and has been extensively used for open ocean missions and under-ice water column survey [15], [22]. For long-range, GPS denied missions, Seagliders rely on long baseline acoustic beacons for georeferenced localization. During a mission in the Davis Strait with a 155.6 km track, the vehicle's dead-reckoned position error was nearly 50% of distance travelled, while the acoustic range-aided localization error was $<$10% of distance travelled. Seagliders have reliably used acoustic range measurements at distances exceeding 400 km from a transmission source in Arctic marginal ice zone (MIZ) environments, where a sound channel is formed by a stratified water layer [23]. In deeper, sub-ice shelf environments, their acoustic range extends to approximately 100 km [22]. While long baseline acoustic beacons have proven to be a robust solution to localizing vehicles on long-range missions when GPS is not available, the beacons must be deployed so that there is always one within range of the vehicle along its flight path. In remote, high latitude environments, this requires deploying moorings or a network of surface vessels to support Seaglider operations. An additional limitation of the Seaglider design is that a hybrid thruster is not supported, which limits their utility to water column profiling or Lagrangian drifting type missions.

The *Slocum* AUG, is a commercially available hybrid-capable AUG design that combines the primary buoyancy drive with an optional thruster and can conduct both vertical water column profiling and constant depth "bathtub" survey missions [24]. The vehicle is designed for modularity and supports a variety of sensor payloads. A Slocum AUG was the first autonomous vehicle to cross the Atlantic [3], traveling 7,400 km over a continuous 221 day expedition, and fleets of Slocum Gliders have been operated persistently by the Rutgers University Coastal Ocean Observation Lab to collect global observations across continental shelves [25]. The stock flight computer has integrated abort handling routines to improve the safety of operations near sea ice. Friedrichs *et al.* [26] report the deployment of a G2 Slocum Glider under the Nansen Ice Shelf (NIS) in East Antarctica. The glider used the stock flight model to navigate 6.5 km into the NIS cavity, and collected CTD and turbulence data to study eddy-driven heat transport. A Slocum AUG has also been used to map icebergs in the Canadian Arctic [27], and used a Tritech Micron mechanical scanning imaging sonar (MSIS) for mapping and ice-relative navigation.

The hybrid Slocum Glider is an attractive platform for long-range unattended surveys of seafloor and under ice environments, given its man-portable size, unmatched range in buoyancy-driven, low-power flight, and proven ability to fly efficient neutral buoyancy "bathtub" missions at constant depth by utilizing a thruster for propulsion. However, without frequently surfacing to obtain GPS fixes or using external acoustic navigation beacons [28], the glider's localization estimate can accumulate large errors during transit. This error accumulates especially quickly during constant-depth "bathtub" missions, where the stock flight dynamics model is poorly determined.

Improved AUG dead-reckoning accuracy has been demonstrated in post-processing by incorporating high fidelity vehicle dynamics models [29], regional ocean models [30], and Doppler velocity log (DVL) bottom-lock estimates to account for ocean currents [31]. Water column acoustic Doppler current profile (ADCP) data can be used without bottom-lock, regional ocean models, or a vehicle dynamics model to improve dead-reckoning accuracy. This method has been described and demonstrated for post-processed AUG localization in [1], [6], [32]. We extend this work by integrating this localization method as an embedded process for real-time AUG navigation correction, and demonstrate a system architecture for navigating the AUG from a backseat computer interfaced with the stock flight controller. Real-time methods for AUV dead-reckoning, such as [33], typically assume vehicle pitch and roll-stability and rely on models informed by a tactical grade IMU to compensate for the periodic dropout of DVL bottom-lock data. In contrast, our real-time method accommodates AUG pitch and roll instability without requiring a tactical grade IMU, vehicle model, or periodic bottom lock. We validate our system in field trials across diverse marine environments, including a shallow bay during

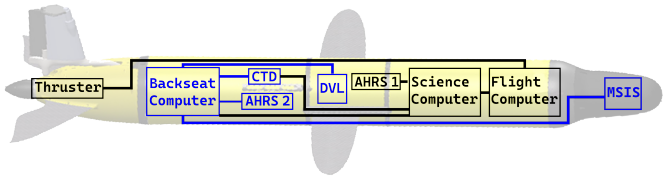

Fig. 2: Key hardware components of *EPIC-DAUG*, our modified 1000 m depth rated G3 Slocum Glider [34]. The backseat computer (Raspberry Pi4) directly communicates with the sensors highlighted in blue (downward facing DVL, AHRS, CTD, and a 360^o mechanically scanned imaging sonar) The backseat computer receives other glider system data through a serial link to the stock science computer. The backseat computer also sends waypoint updates and flight directives during active missions through this serial link. This AUG uses modified wings and added tail stabilizers to improve hydrodynamic efficiency. The thruster is an experimental design that provides a greater velocity envelope for the AUG than a stock thruster.

intense tidal shifts, across a shelf break, and in shallow waters of the Arctic MIZ.

III. Method

A. Hardware Architecture

The hardware architecture of our modified G3 Slocum Glider, summarized in Figure 2, is designed to improve the glider's utility for long-range survey missions in confined (e.g. shallow) as well as open ocean environments. An ideal survey platform can maintain a consistent depth profile with minimal pitch angles and good control authority. While these attributes match the flight dynamics of conventional AUVs and ROVs, the standard "yo-yo" vertical profiles of AUGs do not exhibit these characteristics. Slocum Gliders are fitted with either a shallow (200 m) or deep (1000 m) rated buoyancy drive, depending on the intended operating scenario [34]. Shallow drives have a faster response time, enabling shorter inflections when operating in narrow depth bands or flying at constant depth. The slower dynamics of deep buoyancy drives are not well suited for efficient shallow water or narrow depth band flight. To improve flight dynamics in these conditions with the deep buoyancy drive, our glider uses modified lifting surfaces and a custom thruster. This custom thruster also widens our glider's operating speed envelope from 1.15 to 2 m/s, and enables horizontal flight speeds with "bathtub" profiles in excess of 1.5 m/s [34].

The AUG is instrumented with a Sea-Bird Scientific CTD sensor and a Teledyne RDI Pathfinder 600 kHz phased array Doppler Velocity Log (DVL). We integrate a Raspberry Pi4 computer, which we call the backseat driver (BSD), to interface with modular sensor payloads, run our autonomy stack, and send waypoint updates to improve upon the stock flight computer's navigation. The CTD communicates directly with both the stock science computer and the BSD over serial. Since the stock science computer records data at a limited rate, the DVL is directly connected to the BSD for higher collection and processing rates. To support our backseat navigation method and enable accurate projection of active sensors into the world frame while the glider is pitching, we integrate a high-rate Sparton M2 altitude and heading reference system (AHRS) that directly communicates with the BSD. For surveying, we integrated a 700 kHz Tritech Micron mechanically scanned imaging sonar (MSIS) that directly communicates with the BSD. The rotation range of the MSIS can be configured in software, enabling use for a variety of surveying tasks (e.g., upward-looking sea surface or ice mapping, downward-looking seafloor mapping). For our field trials, we configured the sonar to have a maximum range of 50 m. The imaging sonar is passively stabilized within the nose cone to maintain a horizontal axis of rotation regardless of vehicle pitch, while preserving hydrodynamic efficiency.

TABLE I: This table provides estimates of the average transport cost for our modified glider under three operating modes – deep transit, coastal transit, and survey mode. The maximum range in each flight mode is estimated for rechargeable secondary lithium ion batteries as well as lithium primary batteries. We note that these chemistries can lose significant capacity during low-temperature operation, so these estimates represent an optimistic upper range limit.

	Deep Transit	Coastal Transit	Survey Mode
Depth Band	1000 m	150 m	10 m
Transport Cost (Joules/m)	3 J/m	10 J/m	29 J/m
Average Hotel Load (W)	0.35W	0.35W	15W
Velocity	0.25 m/s	0.69 m/s	0.9 m/s
Endurance [3.2 kWh]	4300 h	460 h	120 h
Range [3.2 kWh]	3800 km	1200 km	400 km
Endurance [12 kWh]	16000 h	1700 h	460 h
Range [12 kWh]	14000 km	4300 km	1500 km

The *EPIC-DAUG* vehicle utilizes rechargeable lithium-ion secondary batteries. For longer-range missions, the glider can be fitted with higher energy density lithium primary batteries. In Table I, we present the measured transport cost, as defined in [6], and estimated ranges of the glider in three different operating modes – deep transit, coastal transit, and survey mode. For open ocean transits, we assume the glider operates with non-necessary components powered down and surfaces for 5 minutes every 12 to 16 hours to communicate mission updates, transfer data, and acquire GPS fixes to constrain navigation. When transiting in deep water, the glider can exploit its 1000 m operating depth for maximum efficiency by using its buoyancy-driven propulsion exclusively. When transiting in shallow coastal waters ($100 - 200$ m), it becomes more advantageous to use a combination of buoyancy and thruster-driven propulsion. When running bathtub profile surveys, we assume that all hardware components are active and that the operating depth band is restricted by sensor requirements, increasing overall power demand and making exclusively thruster-driven propulsion the most efficient.

The optimal speed and hybrid propulsion mix for these operating modes are highly dependent on hotel load, depth band and water column currents [6]. Our system is capable of seamless transition between these different modes of op-

eration, so endurance and range for any given mission would factor in time spent in each of these modes. When fitted with primary cell lithium batteries, the estimated maximum range of the glider is similar to other long-range AUV platforms (i.e., an Autosub or Tethys) while still remaining 2-person portable. In the deep-ocean, using a buoyancy-driven transit mode with all non-essential hardware components powered down, we estimate that the maximum range of the glider would exceed the 6000 km range for the ALR6000 and the 2000 km range for the Tethys AUV. When operating in the thruster-driven survey mode with all hardware components active (representing a 15W hotel load), we estimate the maximum range to exceed 1500 km. We anticipate improvements to the power efficiency during survey mode in planned future modifications, which will further extend the endurance and range of the vehicle.

B. Software Architecture

EPIC-DAUG's stock flight and science computers remain largely unmodified, and the glider can be operated following standard mission procedures without powering the BSD computer or any of the additional components. The only modification to the stock system is the addition of an external control proglet on the science computer that enables the BSD to communicate with the science computer over a serial interface to transfer files, enable and disable glider behaviors, and read and write sensors. The BSD autonomy stack is implemented in ROS, and the interface to the proglet on the science computer is based on a ROS package. This interface exposes sensor data from the science computer as ROS topics, and sending commands from the BSD to the flight computer is facilitated through ROS service calls.

A block diagram of the BSD autonomy stack is shown in Figure 3. The system includes drivers for each of the interfaced sensors. The sensor data is piped into a navigation node that implements a DVL based odometery process, DVL-odo, described previously in [1], based on [6] and [32]. We implement a mission controller node to monitor the backseat navigation estimate and status reported from the frontseat system, including the flight computer's estimated global position. The mission controller uses the external control node to communicate with the science computer and adjust the glider's flight behavior based on the backseat navigation process. This control node can adjust the glider's climb and dive pitch angles, flight depth band limits, target waypoint coordinates or heading, buoyancy pump set-point and limits, and thruster power.

C. Mission Architecture

In this work, we focus on a specific implementation of an experimental backseat mission controller, which we term "carrot following", in which a stock glider mission and flight parameters are configured as normal, but the BSD feeds the flight computer the target waypoints and continually adjusts for drift in the frontseat navigation estimate. The BSD stores a list of the target waypoints for a mission, iterating to the next waypoint only when a minimum distance threshold is met

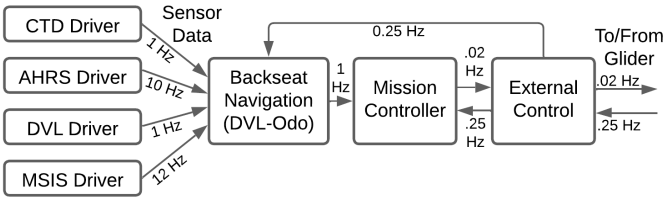

Fig. 3: Diagram of the core ROS nodes running on the backseat driver. The central node of the system is the backseat navigation process, which subscribes to topics published by ROS drivers for each of the interfaced sensors as well flight status topics from the frontseat, published by the external control node. The mission controller publishes directives to the flight computer based on the current backseat navigation estimate. The rate and direction of messages between nodes are noted by the connecting arrows.

between the backseat navigation estimated position and the current target waypoint. The BSD regularly updates the target waypoint sent to the flight computer, based on the discrepancy between the backseat navigation estimated global position and the reported global position from the frontseat. The waypoint updates sent to the flight computer act like carrots leading the glider in its internal reference frame to the true waypoint position, as estimated by the backseat navigation process. Figure 4 illustrates how the frontseat waypoint updates or carrots are calculated. We note that relative position estimates and waypoint updates are made in latitude and longitude coordinates to minimize any inaccuracies due to local Euclidean coordinate projections. This is particularly relevant in high latitude zones. We define the following variables representing global latitude and longitude positions:

$\mathbf{W}$ = True target waypoint
$\mathbf{F}_t$ = Frontseat position estimate at time t
$\mathbf{B}_t$ = Backseat position estimate at time t
$\mathbf{T}_t$ = Frontseat updated target waypoint (carrot) at time t

The waypoint update at time t is calculated as

$$\mathbf{T}_t = \mathbf{W} + (\mathbf{F}_t - \mathbf{B}_t). \tag{1}$$

As a practical point of implementation, we note that if the BSD tries to send data to the frontseat too frequently, we found that a memory buffer related to the serial comms on the frontseat computer can overflow and crash the system. We limit the frequency of waypoint updates to 50 seconds, which we found to be well within the margin of safety.

While operating glider missions in open ocean environments is relatively straightforward, operations in potentially surface-denied ocean environments such as under ice shelves or in MIZ regions is risky for the vehicle. The frontseat vehicle control has built in ice handling behaviors that trigger when the glider tries to surface but senses it cannot due to a surface blockage. We leverage these behaviors with customizations for Arctic MIZ operations. Our backseat-frontseat mission control architecture is implemented such that these abort scenarios

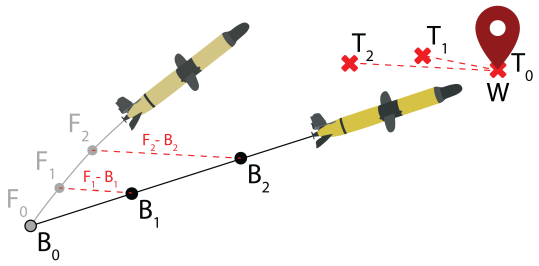

Fig. 4: Illustration of the "carrot following" backseat mission controller. The updated waypoint position (carrot) sent to the flight computer is calculated as the true waypoint position plus the offset between the frontseat and backseat global position estimates. In this way, the vehicle is always steered towards the true waypoint as estimated by the backseat navigation process.

are handled completely by the frontseat system, which have proven reliability over decades of Slocum Glider operations.

Figure 5 provides a block diagram of the overall mission architecture with the carrot-following backseat mission controller (BMC). In general, we configure the frontseat to surface whenever it reaches within a threshold range of a target waypoint. If a surface event is desired at a waypoint, the BMC is configured to steer the frontseat to within its threshold surfacing range. If a surface event is not desired at a waypoint, the BMC is configured to iterate to the next waypoint before the frontseat surfacing threshold is triggered. If the glider gets stuck in place at some depth while in mission, and the ice handling behaviors are active, it is assumed that the glider has gotten caught on thick ice, and a freewiggle behavior is triggered, in which the glider tries to free itself by executing a steep dive and climb cycle repeatedly, until it senses it is unstuck and then continues on its mission. In the case of any mission failure that causes the glider to abort, an under ice surfacing process is triggered, in which the glider sequences a series of behaviors designed to lead it back to open water, should the surface be blocked by ice. If the glider senses it is stuck near the surface, but it cannot connect to satellite comms within a designated period, it assumes that it is trapped under thin ice, and a breadcrumb mission is activated that steers the glider back through a series of waypoints where it last had surface GPS fixes. If the glider fails to surface after completing the breadcrumb mission, a recovery mission is activated that, in stock configuration, will steer the glider to a designated waypoint and hold station there for rescue. If the glider senses it is trapped under thick ice while trying to surface, it will first initiate the freewiggle behavior before sequencing the breadcrumb and finally the recovery mission. For operations in the Arctic MIZ, we kept the freewiggle and breadcrumb behaviors as designed in the stock version of the frontseat controller, but modified the recovery mission to continuously drive the glider South towards known open ocean, while periodically trying to surface. We considered this generally safer than leaving the glider potentially stuck under some unknown location in the ice field. Although the under ice abort behavior was never triggered during active missions, we ran tests in which we artificially triggered the full sequence of under ice abort behaviors and verified the glider behaved as intended.

IV. Field Trials

We conducted several field trials to evaluate the proposed AUG architecture. These field trials occurred (A) in Eastern Caribbean coastal areas near La Paguera, Puerto Rico and (B) off the shelf break south of Cabo Rojo in Puerto Rico, (C) in Buzzards Bay, MA, and (D,E,F) in the Arctic Ocean's Beaufort Sea MIZ, northeast of Prudhoe Bay, AK. The AUG was operated in survey mode, where the vehicle records data from all sensors while following a "bathtub" profile. In this operational mode, the vehicle buoyancy is kept neutral, and the vehicle makes minor corrections to its pitch to stay within a narrow depth band. For evaluation, the datasets are segmented into individual legs, where each leg contains the data collected between subsequent surface GPS fixes. An overview of the collected datasets, along with the dates they were collected, is presented in Table II and Figures 6 and 7.

TABLE II: Summary of the field trials and collected datasets. For each location, we list the number of waypoints used and the number of trials (legs) conducted. We also include some brief notes about salient environmental conditions.

Location	Date	Wpts	Legs	Comments
PR (A)	20NOV22	4	11	Shelf break Drift: 0.05 m/s W[1] Wind: 8 kn SE [35]
PR (B)	31MAR23	4	17	Coral head Drift: 0.05 m/s NW[1] Wind: 9 kn N [35]
BB (C)	11JUL23	2	3	Drift: 0.2 m/s NE[1] Wind: 7 kn WNW [36] Waves: 1-1.5m [35]
AK (D)	02AUG23	3	4	Drift: 0.4 m/s SSE[1] Wind: 8 kn NNE [36]
AK (E)	03AUG23	2	2	Drift: 0.3 m/s SE[1] Wind: 13 kn NW [36]
AK (F)	04AUG23	5	3	Drift: 0.2 m/s NE[1] Wind: 14 kn ENE [36] Waves: 1-2.5 m[2]

PR: Puerto Rico; AK: Alaskan Arctic; BB: Buzzards Bay, MA
[1] Estimated from GPS measurements with glider at surface
[2] Estimated from day-of observations

A. Navigation Results

We operated the glider with the carrot following type backseat mission controller for the field tests in Buzzards Bay (C) and Beaufort Sea (D-F). For the earlier field trials conducted in Puerto Rico, we operated the glider with completely frontseat controlled missions, and the performance of the DVL-Odo navigation method for these trials compared to the frontseat internal navigation has been previously reported in [1].

In Table III, we report the navigation performance of the BMC guided missions in comparison to the frontseat internal navigation. The horizontal distance travelled for a

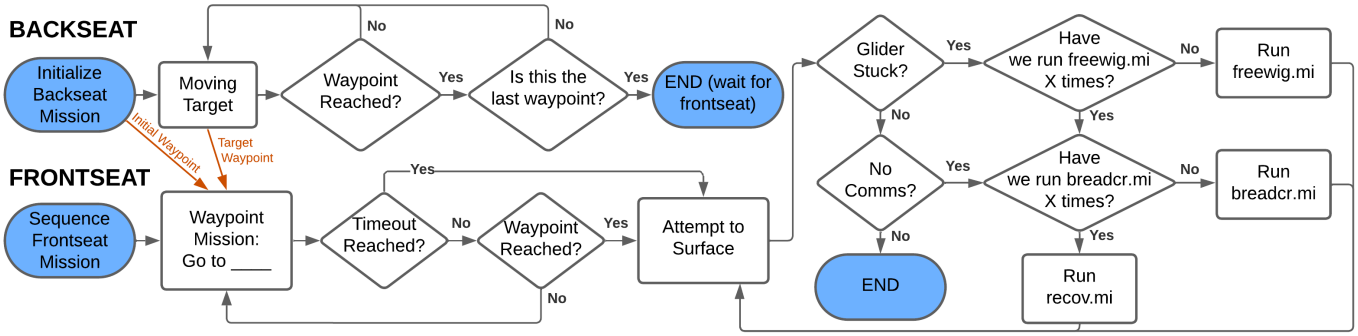

Fig. 5: Diagram of our "carrot following" type mission architecture, where the frontseat sequences a mission as normal, and the backseat mission controller feeds waypoint updates to the frontseat. Also shown is the under ice surfacing behavior, which is also triggered whenever there is an abort for any reason.

leg is estimated by taking a sum over the deltas between sequential DVL-Odo position estimates, excluding discontinuous "jumps" in the data due to corrections applied by the DVL-Odo process. The navigation error is then computed by taking the distance between the first valid GPS fix after the glider surfaces and the last recorded odometry position estimate before surfacing. The error is also reported as a percent of the horizontal distance travelled.

The frontseat's internal navigation process uses a model-based position estimation approach, which is optimized for a stock vehicle completing "yo-yo" profiles with large pitch angles during transit. However, the glider used in our operations features a modified thruster and wings, and was operated along "bathtub" trajectories with small pitch angles. These discrepancies between the model's assumptions and the actual operational conditions result in a notably large error within the frontseat's navigation estimate.

Across all BMC guided missions, our system achieved an average position error of 11% of distance travelled, compared to the average frontseat internal navigation error of 44% of distance travelled. It is noteworthy that the navigation percent error did not correlate with leg length, but seemed, rather, to be relatively consistent across legs that occurred on the same day. In particular, there is a strong correlation between the direction of the surface current and the navigation error for datasets C, D, and E. This implies that the variability in the navigation error may be due to error in GPS-estimated surface drift prior to each dive, and not the navigation processes used while submerged.

While most of the missions were operated as simple "go to" missions with a single target waypoint, two of the missions in the Arctic (F1 and F3) were configured to have the glider achieved an intermediate waypoint and then turn and traverse to the final waypoint without surfacing. It is also noteworthy that despite involving significant subsurface turns, both of these missions maintained relatively low navigation error.

Of the legs that ended normally (i.e., the glider attempting to surface at the waypoint), the average *Distance to Waypoint* was 200 m. However, it's worth noting that the glider was instructed to surface as soon as it was within a set distance to the waypoint (200 m for dataset C, 150 m for datasets D, E, F). As illustrated in Figure 7, this consistently caused the glider to surface ∼150-200 m before reaching the actual waypoint. Reducing the waypoint radius should improve the glider's ability to achieve the desired waypoint goal more precisely.

TABLE III: Navigation performance for backseat guided missions. The distance is the estimated horizontal distance travelled for the leg. We report the error for both the backseat (BS) and frontseat (FS) navigation processes. The error is measured as the distance between the first valid GPS fix after a leg and the last odometery position estimate before getting the fix. The error is also reported as a percent of the distance travelled. The waypoint reached threshold was set to 200 m for dataset C and 150 m for the other datasets.

Leg	Wpt Goals	Dist (m)	BS Error (m, %)	FS Error (m, %)	Dist to Wpt (m)
C1	1	750	86 (12%)	413 (55%)	162*
C2	2	576	53 (9%)	152 (26%)	182
C3	1	567	35 (6%)	356 (63%)	138
D1	1	986	131 (13%)	454 (46%)	1097*
D2	1	1274	249 (20%)	666 (52%)	267
D3	2	1375	257 (19%)	318 (23%)	234*
D4	3	2089	141 (7%)	330 (16%)	146
E1	1	2144	343 (16%)	1743 (81%)	378
E2	2	3135	249 (8%)	2461 (79%)	261
F1	1,2	1617	129 (8%)	485 (30%)	238
F2	3	409	22 (5%)	131 (32%)	123
F3	4,5	989	37 (4%)	270 (27%)	67

*The AUG surfaced due to a communications interval timeout abort before reaching the waypoint for these legs

B. *Survey Results*

The onboard DVL-Odo process with the backseat driven navigation enables accurate georeferenced sonar acoustic survey of the seafloor and the ocean surface, including ice-covered regions. Here we report experimental results with our system for bathymetric mapping of coastal Puerto Rico and Alaska, and for sea-ice coverage characterization in the Arctic MIZ. A sound speed correction, based on CTD data, is applied

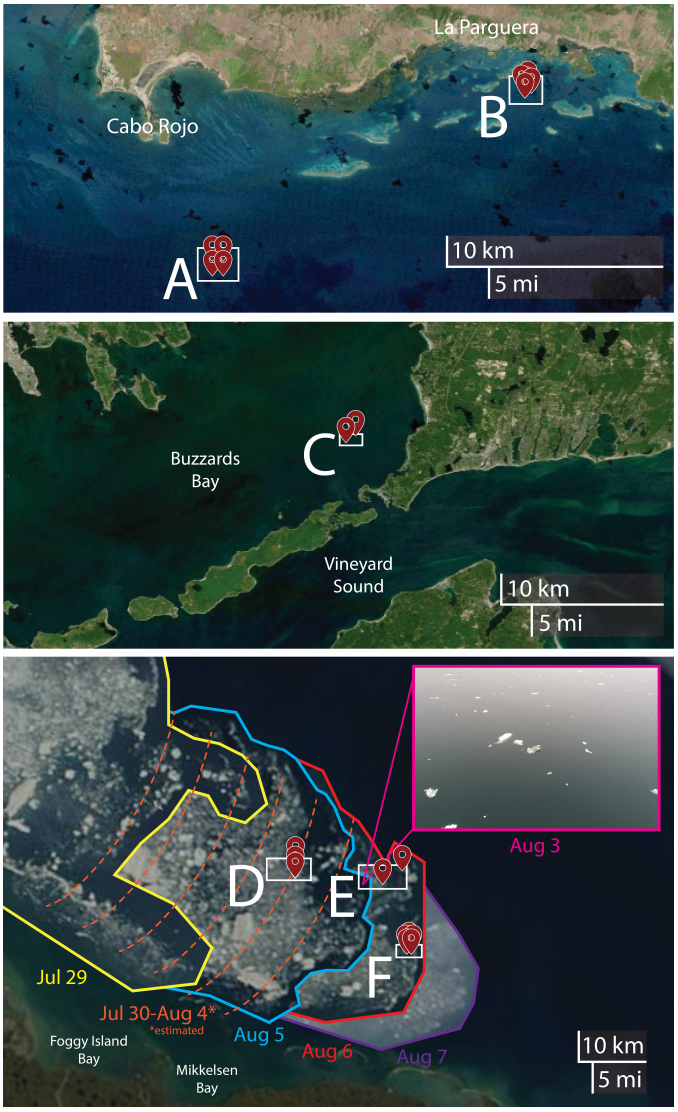

Fig. 6: Waypoint locations for the collected datasets in (top) Puerto Rico, (middle) Buzzard's Bay, and (bottom) Arctic, with imagery from the NASA Worldview application [37]. In the Arctic, the drift ice near the areas of operation are visualized as a time series composite image based on true color data from Terra/MODIS data [38] on July 29th and from August 5-7th, for reference. (Ice imagery is not available July 30th-August 4th due to cloud cover). (bottom inset) Drone photograph of ice cover at start position of Leg E1 on August 3rd, 2024

to both the MSIS and DVL range measurements. Additionally, a static offset is applied to the depth measurements to account for the initial offset of the pressure sensor. The bathymetric results are derived from the online DVL-Odo process and thus do not include post-process corrections to the glider's estimated track based on resurfacing GPS fixes.

[1]During legs C1 and D3, the glider stopped recording CTD data and surfaced before reaching the waypoint because the mission was configured with overly conservative limits on dive duration.

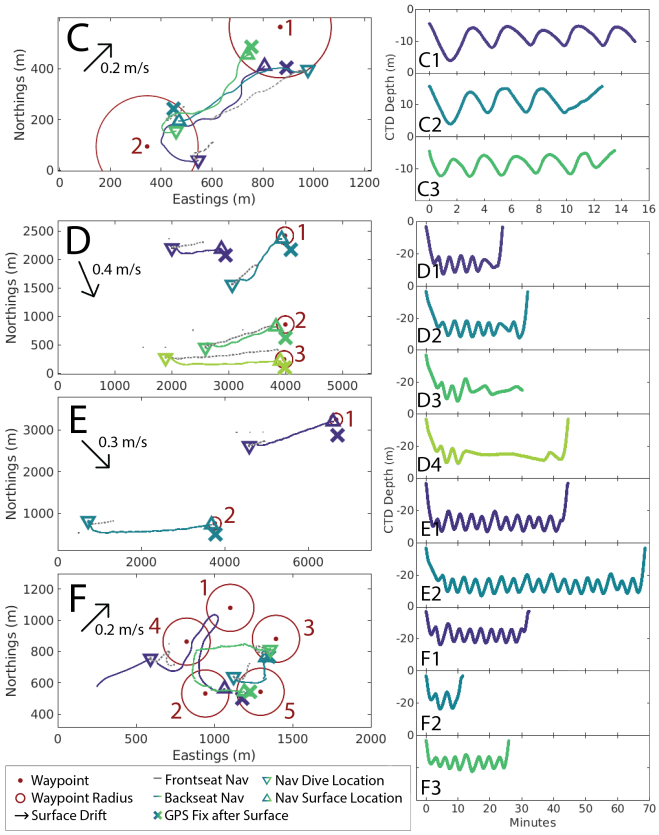

Fig. 7: (left) Navigation Results and (right) dive profiles per leg[1] for datasets collected in Buzzard's Bay (C) and the Beaufort Sea (D,E,F). For each leg in the dataset, the glider's estimated trajectory based on both the frontseat (grey) and backseat (colored) odometry are shown. For reference, the figure also illustrates the glider's dive and surface locations, the measured surface drift, and the first GPS fix after surfacing per leg. The waypoint goals for each leg are labelled with the corresponding leg color (some legs in F had multiple waypoint goals before surfacing).

For the Puerto Rico datasets, the bathymetry maps were created by projecting the range data from the DVL and the maximum intensity ranges from the MSIS sonar into the global reference frame using position estimates from the DVL-Odo process. We overlay the results from these sensor projections with maps of known bathymetry recorded from aerial LiDAR surveys. The results of this comparison are shown in Figure 8. The projected bathymetric measurements are in close agreement with the prior maps for the shelf break. In addition, for one of the legs, the glider transited over a known large coral head, which also aligns well with the prior bathymetric maps.

In the Arctic MIZ of the Beaufort Sea we conducted simultaneous bathymetric survey with the DVL and upward facing ice-profiling with the MSIS. For these datasets, the MSIS was configured with a maximum range of 50 m and an upward looking sweep range. The bathymetric map was

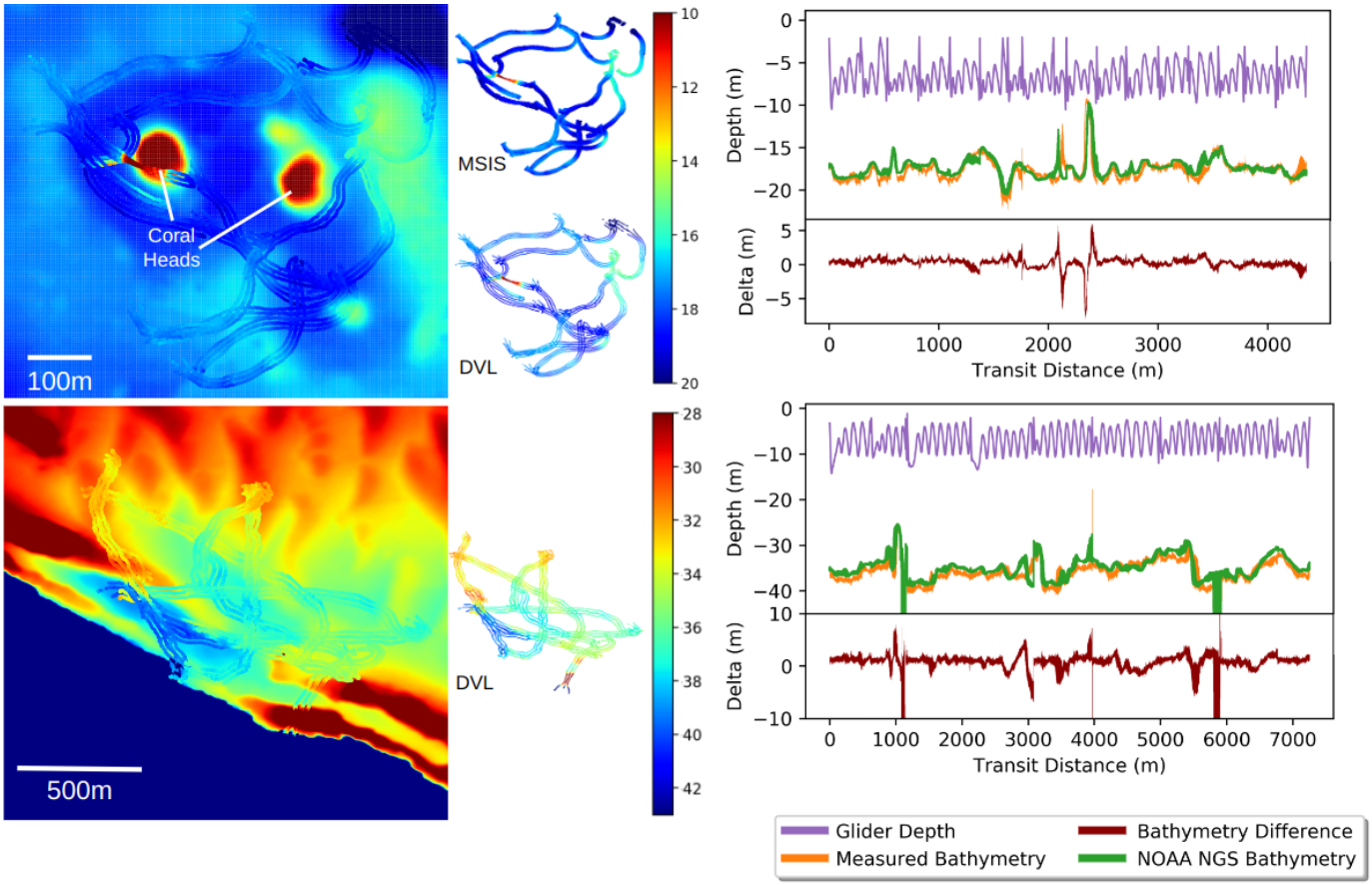

Fig. 8: DVL (Top, Bottom) and MSIS (Top) survey results from our AUG traversing over a coral head and shelf break, overlaid on 2015 aerial NOAA NGS Topobathy LiDAR gridded at 2 m [39]. (Right) Plots showing the AUG depth profile and the difference between the AUG and LiDAR bathymetry data show good agreement between both datasets. (Top) Delta Mean: 0.29, Median: 0.35, Std: 0.78. (Bottom) Delta Mean: 0.53, Median: 1.07, Std: 3.75. Displayed ranges for the bathymetry and deltas are truncated to illustrate bathymetry variations on the shelf with more detail.

computed using the position estimates from the real-time DVL-Odo process. As illustrated in Figure 9, ice scours are visible in the bathymetry near detected surface ice regions. Although there is a $\sim$3m discrepancy between the AUG's estimate of ocean floor depth and the IBCAO map, the map's gridding is based on heavily interpolated data of varying quality [40]. Furthermore, the accuracy of the AUG's estimates were verified using the surface support vessel's depth sounder logs.

To process MSIS returns for ice, acoustic multipath from the nose cone was filtered out, and the data was thresholded and segmented to identify ice signals. The process for ice detection signal processing has been preliminarily described in [6] and will be detailed further in a future publication. In Figure 9, positive ice detections are visualized as spheres scaled according to the intensity of the acoustic return, which correlates to ice thickness. These detected ice features are also projected into the global reference frame based on the real-time DVL-Odo position estimates.

We note that in both the ice profiling and bathymetric survey data, the acoustic returns are projected into the global frame with consistent depth, illustrating that the active pitching and depth variations of the glider during survey profiling do not impact the quality of the survey data with our proposed system and demonstrating the suitability of our system for conducting precise acoustic surveys.

V. Discussion & Conclusion

These field experiments demonstrate that our improved navigation process combined with our real-time backseat mission controller enables accurate georeferenced bathymetric and ice profiling surveys with a low-power AUG. This system extends the potential range of unattended surveys an order of magnitude beyond conventional AUV systems and is competitive in maximum range with other long-range AUVs that are significantly more costly or logistically complex to operate. Assuming a maximum viewing angle of $\pm 45^{\circ}$ and a 75 m slant range, the theoretical maximum sea-ice survey area using this AUG method is 150 km^2 when equipped with lithium primary batteries. It can efficiently transit long-range in both deep open ocean and in coastal waters as shallow as 10 m depth, while seamlessly transitioning to bathtub profile survey

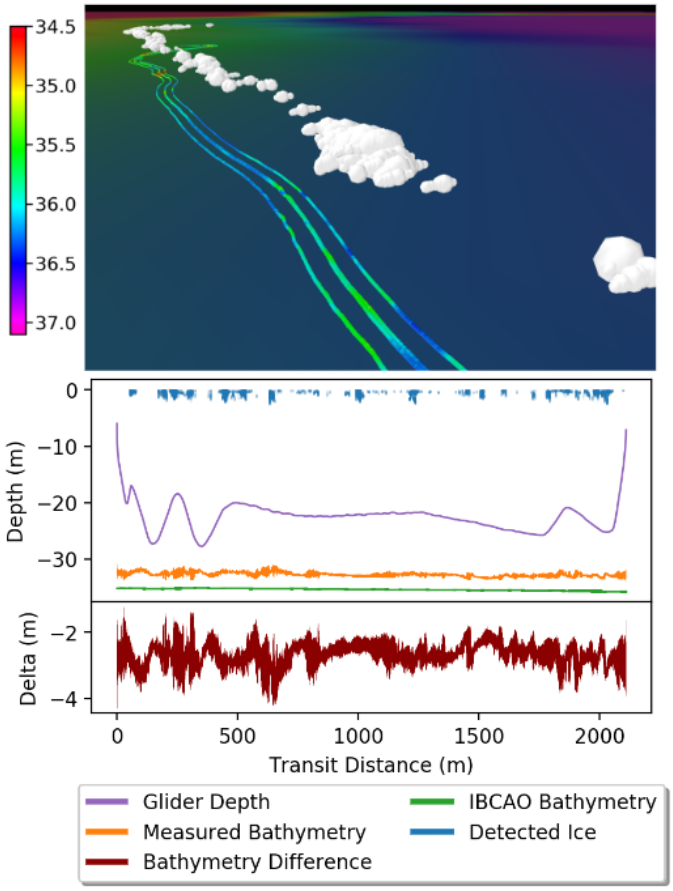

Fig. 9: Results from simultaneous bathymetric and ocean surface ice mapping using the DVL and MSIS sonar (extent of the shown vehicle track is approximately 1.3 km). The MSIS data, collected using an upward looking +/- 10 deg sweep across the vehicle track, are used to identify ice distribution. The downward looking DVL ocean floor acoustic returns from each Doppler beam appear as colored icons below the MSIS data. Discrete ice floes (white) are visible at the sea surface, along with ocean floor scours (blue) and ridges (red) extending in a generally NW-SE orientation. The underlay shows IBCAO bathymetric data (Version 4.2.13) [40] gridded at its native 200m horizontal resolution.

mode at any point in the mission. This capability enables new types of missions where AUGs could be launched from shore, travel thousands of kilometers to an area of interest, conduct surveys, and return to the launch point in a fully unattended manner.

We recognize that our evaluation is limited to the relatively short "proof-of-concept" survey legs that were completed in lieu of long-range (hundreds of kilometer) missions. This approach was largely motivated by balancing the risk of using a prototype vehicle, with the numerous time varying constraints of Arctic operations which were exacerbated by logistics challenges caused by the COVID pandemic. For example, in the Arctic MIZ, we originally planned to demonstrate

Fig. 10: During field trials in the Arctic MIZ, we observed ice floes with grounded pressure ridges along the edge of the ice sheet in >30 m water depth, illustrating the challenges and risks of operating in these extreme environments.

longer under-ice missions. However, during deployments, we struggled to find open water deeper than 30 m to safely deploy the vehicle from a small boat, and observed large grounded ice floes in areas with >30 m water depth along the ice sheet edge that posed a significant entrapment risk to the vehicle (Figure 10). These observations illustrate the general complexity and risks of operating in remote environments, which must be carefully considered when planning long-range unattended missions. Our results in this paper show promise in enabling safe AUG operations in a variety of challenging environments, and we plan to conduct operations using the architecture described here to demonstrate long-range survey missions in future work.

VI. Acknowledgments

The authors gratefully acknowledge the science team members Ted Maksym and Angelos Mallios, Professor Roy Armstrong and Orlando Espinosa (captain of the *R/V Gaviota*) from the University of Puerto Rico, and Arthur Schwartz (captain of the *R/V Ukpik*) for their invaluable support in conducting the field operations essential for this work.

References

[1] G. Billings, A. Phung, and R. Camilli, "Dvl-based odometry for autonomous underwater gliders," in *2023 IEEE/RSJ International Conference on Intelligent Robots and Systems (IROS)*, IEEE, 2023, pp. 9910–9917.

[2] H. Stommel, "The slocum mission," *Oceanography*, vol. 2, no. 1, pp. 22–25, 1989.

[3] S. Glenn *et al.*, "The trans-atlantic slocum glider expeditions: A catalyst for undergraduate participation in ocean science and technology," *Marine Technology Society Journal*, vol. 45, no. 1, pp. 52–67, 2011.

[4] L. M. Smith *et al.*, "The ocean observatories initiative," *Oceanography*, vol. 31, no. 1, pp. 16–35, 2018.

[5] D. L. Rudnick, R. E. Davis, C. C. Eriksen, D. M. Fratantoni, and M. J. Perry, "Underwater gliders for ocean research," *Marine Technology Society Journal*, vol. 38, no. 2, pp. 73–84, 2004.

[6] Z. Duguid and R. Camilli, "Improving resource management for unattended observation of the marginal ice zone using autonomous underwater gliders," *Frontiers in Robotics and AI*, vol. 7, p. 579 256, 2021.

[7] C. L. Kaiser *et al.*, "The design and 200 day per year operation of the autonomous underwater vehicle sentry," in *2016 IEEE/OES Autonomous Underwater Vehicles (AUV)*, IEEE, 2016, pp. 251–260.

[8] C. R. German *et al.*, "A long term vision for long-range ship-free deep ocean operations: Persistent presence through coordination of autonomous surface vehicles and autonomous underwater vehicles," in *2012 IEEE/OES Autonomous Underwater Vehicles (AUV)*, IEEE, 2012, pp. 1–7.

[9] W. Weeks, *On sea ice*. University of Alaska Press, 2010.

[10] L. D. Barker *et al.*, "Scientific challenges and present capabilities in underwater robotic vehicle design and navigation for oceanographic exploration under-ice," *Remote Sensing*, vol. 12, no. 16, p. 2588, 2020.

[11] K. Reeve, O. Boebel, T. Kanzow, V. Strass, G. Rohardt, and E. Fahrbach, "A gridded data set of upper-ocean hydrographic properties in the weddell gyre obtained by objective mapping of argo float measurements," *Earth System Science Data*, vol. 8, no. 1, pp. 15–40, 2016.

[12] A. D. Bowen *et al.*, "Design of nereid-ui: A remotely operated underwater vehicle for oceanographic access under ice," in *2014 Oceans-St. John's*, IEEE, 2014, pp. 1–6.

[13] R. Francois and W. Nodland, "Unmanned arctic research submersible system development report, phase i," Tech. Rep., 1971.

[14] G. Williams *et al.*, "Thick and deformed antarctic sea ice mapped with autonomous underwater vehicles," *Nature Geoscience*, vol. 8, no. 1, pp. 61–67, 2015.

[15] C. M. Lee, J. Thomson, M. I. Zone, and A. S. S. Teams, "An autonomous approach to observing the seasonal ice zone in the western arctic," *Oceanography*, vol. 30, no. 2, pp. 56–68, 2017.

[16] J. Thorleifson *et al.*, "The theseus autonomous underwater vehicle. a canadian success story," in *Oceans' 97. MTS/IEEE Conference Proceedings*, IEEE, vol. 2, 1997, pp. 1001–1006.

[17] D. Roper *et al.*, "Autosub long range 6000: A multiple-month endurance auv for deep-ocean monitoring and survey," *IEEE Journal of Oceanic Engineering*, vol. 46, no. 4, pp. 1179–1191, 2021.

[18] A. B. Phillips *et al.*, "Autosub long range 1500: A continuous 2000 km field trial," *Ocean Engineering*, vol. 280, p. 114 626, 2023.

[19] S. McPhail, R. Templeton, M. Pebody, D. Roper, and R. Morrison, "Autosub long range auv missions under the filchner and ronne ice shelves in the weddell sea, antarctica-an engineering perspective," in *OCEANS 2019-Marseille*, IEEE, 2019, pp. 1–8.

[20] B. W. Hobson, J. G. Bellingham, B. Kieft, R. McEwen, M. Godin, and Y. Zhang, "Tethys-class long range auvs-extending the endurance of propeller-driven cruising auvs from days to weeks," in *2012 IEEE/OES autonomous underwater vehicles (AUV)*, IEEE, 2012, pp. 1–8.

[21] C. C. Eriksen *et al.*, "Seaglider: A long-range autonomous underwater vehicle for oceanographic research," *IEEE Journal of oceanic Engineering*, vol. 26, no. 4, pp. 424–436, 2001.

[22] S. E. Webster, C. M. Lee, and J. I. Gobat, "Preliminary results in under-ice acoustic navigation for seagliders in davis strait," in *2014 Oceans-St. John's*, IEEE, 2014, pp. 1–5.

[23] S. E. Webster, L. E. Freitag, C. M. Lee, and J. I. Gobat, "Towards real-time under-ice acoustic navigation at mesoscale ranges," in *2015 IEEE International Conference on Robotics and Automation (ICRA)*, IEEE, 2015, pp. 537–544.

[24] L. Cooney, "Expanding the capabilities of the slocum glider," in *OCEANS 2016 MTS/IEEE Monterey*, IEEE, 2016, pp. 1–5.

[25] J Graver *et al.*, "Rucool operational oceanography: Using a fleet of autonomous ocean gliders," in *AGU Spring Meeting Abstracts*, vol. 2007, 2007, OS23H–08.

[26] D. M. Friedrichs *et al.*, "Observations of submesoscale eddy-driven heat transport at an ice shelf calving front," *Communications Earth & Environment*, vol. 3, no. 1, p. 140, 2022.

[27] M. Zhou, R. Bachmayer, and B. deYoung, "Mapping the underside of an iceberg with a modified underwater glider," *Journal of Field Robotics*, vol. 36, no. 6, pp. 1102–1117, 2019.

[28] L. Freitag, K. Ball, J. Partan, P. Koski, and S. Singh, "Long range acoustic communications and navigation in the arctic," in *OCEANS 2015-MTS/IEEE Washington*, IEEE, 2015, pp. 1–5.

[29] P. Wang, P. K. Singh, and J. Yi, "Dynamic model-aided localization of underwater autonomous gliders," in *2013 IEEE International Conference on Robotics and Automation*, IEEE, 2013, pp. 5565–5570.

[30] R. N. Smith, J. Kelly, Y. Chao, B. H. Jones, and G. S. Sukhatme, "Towards the improvement of autonomous glider navigational accuracy through the use of regional ocean models," in *International Conference on Offshore Mechanics and Arctic Engineering*, vol. 49125, 2010, pp. 597–606.

[31] H. C. Woithe, D. Boehm, and U. Kremer, "Improving slocum glider dead reckoning using a doppler velocity log," in *OCEANS'11 MTS/IEEE KONA*, IEEE, 2011, pp. 1–5.

[32] P. Vrolijk *et al.*, "Using a ladder of seeps with computer decision processes to explore for and evaluate cold seeps on the costa rica active margin," *Frontiers in Earth Science*, vol. 9, p. 601 019, 2021.

[33] S. Arnold and L. Medagoda, "Robust model-aided inertial localization for autonomous underwater vehicles," in *2018 IEEE international conference on robotics and automation (ICRA)*, IEEE, 2018, pp. 4889–4896.

[34] P. T. Ventola, "Developing the next generation of autonomous underwater gliders," M.S. thesis, Massachusetts Institute of Technology, 2022.

[35] N. Oceanic and A. Administration, *National data buoy center*, Accessed on May 9, 2024, 2024.

[36] W. Underground, *Weather underground*, Accessed on May 9, 2024, 2024.

[37] N. E. O. S. Data and I. S. (EOSDIS), *Nasa worldview*, Accessed on May 1, 2024. [Online]. Available: https://worldview.earthdata.nasa.gov, 2024.

[38] U. MODIS Characterization Support Team (MCST). NASA MODIS Adaptive Processing System Goddard Space Flight Center, *Modis 250m calibrated radiances product*, 2017.

[39] N. O. for Coastal Management, *National oceanic and atmospheric administration (noaa) digital coast data access viewer. custom processing of "2015 noaa ngs topobathy lidar: Puerto rico"*, Accessed on Dec 1, 2021, 2015.

[40] M. Jakobsson *et al.*, "The international bathymetric chart of the arctic ocean version 4.0," *Scientific data*, vol. 7, no. 1, p. 176, 2020.